



48th SME North American Manufacturing Research Conference, NAMRC 48 (Cancelled due to COVID-19)

Modal interactions for spindle, holders, and tools

Tony Schmitz^{a,b*}

^aUniversity of Tennessee, Knoxville, 1512 Middle Dr., Knoxville, TN 37996, USA

^bEnergy and Transportation Science Division, Oak Ridge National Laboratory, Oak Ridge, TN 37830, USA

* Corresponding author. Tel.: +1-865-974-6141. E-mail address: tony.schmitz@utk.edu

Abstract

This paper describes the interaction between vibration modes associated with the machine-spindle and those associated with the holder-tool when the holder-tool combination is inserted in the milling machine spindle. It is shown that when the bending natural frequency of the holder-tool is near a machine-spindle natural frequency, there is a combined two mode frequency response (similar to a dynamic absorber) for the assembly that exhibits increased dynamic stiffness over those situations when the interaction is absent. Experimental results are provided. The variation in tool point frequency response with tool extension length is then used to calculate the corresponding stability maps. These maps are evaluated to determine the effect of interactions between machine-spindle and holder-tool modes on milling stability. Conclusions are presented.

© 2020 The Authors. Published by Elsevier B.V.

This is an open access article under the CC BY-NC-ND license (<http://creativecommons.org/licenses/by-nc-nd/4.0/>)

Peer-review under responsibility of the Scientific Committee of the NAMRI/SME.

Keywords: Structural dynamics; machine tools; milling; frequency response function; stability

1. Introduction*

Modal analysis is applied to measure and model the structural dynamics of complex systems [1]. Because an important consideration in milling is the vibration behavior of the cutting tool during material removal, modal techniques are used to study machine-spindle-holder-tool combinations [2]. Important considerations for predicting milling vibration behavior, which can be stable (i.e., exhibits forced vibration only) or unstable (i.e., exhibits either self-excited or period- n bifurcations [3]), are the workpiece material, tool geometry, machining parameters, and structural dynamics [2, 4]. The workpiece material and tool geometry collectively define the relationship between the commanded chip geometry and the cutting force required to shear away the chip. This relationship may be parameterized in the form of a mechanistic cutting force

model or the force may be predicted from the material's constitutive model using finite element analysis. The structural dynamics depend on the machine, spindle, holder, and tool combination, including the tool's extension length from the holder.

Because the tool point receptance (or frequency response function, FRF) is required to select stable machining parameters, identifying it for arbitrary machine-spindle-holder-tool combinations is required. This may be achieved through modal testing techniques, such as impact testing where an instrumented hammer is used to apply the impulsive force input and a linear transducer (typically an accelerometer) is used to measure the corresponding response output. The receptance is the complex, frequency domain ratio of the output to the input. To reduce measurement time, Schmitz and co-authors derived receptance coupling substructure analysis (RCSA) for tool

* Notice: This manuscript has been authored by UT-Battelle, LLC, under contract DE-AC05-00OR22725 with the US Department of Energy (DOE). The US government retains and the publisher, by accepting the article for publication, acknowledges that the US government retains a nonexclusive, paid-up, irrevocable, worldwide license to publish or reproduce the published

form of this manuscript, or allow others to do so, for US government purposes. DOE will provide public access to these results of federally sponsored research in accordance with the DOE Public Access Plan (<http://energy.gov/downloads/doe-public-access-plan>).

point FRF prediction [5-24]. Many other authors have also implemented RCSA for tool point FRF prediction and have added new knowledge to the approach [25-84].

In this paper, RCSA is used to predict tool point receptances for a range of extension lengths with holder-tool bending modes that span multiple machine-spindle bending modes. It is shown that the holder-tool modes interact with the machine-spindle modes to yield increased dynamic stiffness for selected extension lengths. The reported results are contrary to intuition, which would suggest that a shorter tool is always better. The implications of these variations in dynamic stiffness on milling stability are then discussed.

Nomenclature

x_i	lateral displacement at coordinate i
θ_i	rotation at coordinate i
f_i	external harmonic force applied at coordinate i
m_i	external harmonic moment applied at coordinate i
h_{ij}	displacement-to-force receptance between coordinates i and j
l_{ij}	displacement-to-moment receptance between coordinates i and j
n_{ij}	rotation-to-force receptance between coordinates i and j
p_{ij}	rotation-to-moment receptance between coordinates i and j
R_{ij}	component generalized receptance matrix between coordinates i and j
G_{ij}	assembly generalized receptance matrix between coordinates i and j
u_i	generalized component displacement at coordinate i
U_i	generalized assembly displacement at coordinate i
q_i	generalized component force at coordinate i
Q_i	generalized assembly force at coordinate i
K	complex stiffness matrix for non-rigid coupling

2. RCSA

RCSA analytically couples receptance models for the holder and tool to a receptance measurement for the machine-spindle. The required steps are described in the following paragraphs. To begin, consider the tool and holder modeling.

The direct receptances for the free-free beam shown in Fig. 1 due to externally applied harmonic forces $f_1(t)$ and $f_2(t)$, applied at coordinates $x_1(t)$ and $x_2(t)$, and moments $m_1(t)$ and $m_2(t)$, applied at $\theta_1(t)$ and $\theta_2(t)$, are provided in Eq. 1. The corresponding cross receptances are shown in Eq. 2. (Note that the coordinates are listed to consider f or m individually, unlike Eq. 3 which combines the effects). These receptances are used to represent the tool and holder sections prior to coupling.

$$\begin{matrix} x_1 = h_{11}f_1 & x_1 = l_{11}m_1 & x_2 = h_{22}f_2 & x_2 = l_{22}m_2 \\ \theta_1 = n_{11}f_1 & \theta_1 = p_{11}m_1 & \theta_2 = n_{22}f_2 & \theta_2 = p_{22}m_2 \end{matrix} \quad (1)$$

$$\begin{matrix} x_1 = h_{12}f_2 & x_1 = l_{12}m_2 & x_2 = h_{21}f_1 & x_2 = l_{21}m_1 \\ \theta_1 = n_{12}f_2 & \theta_1 = p_{12}m_2 & \theta_2 = n_{21}f_1 & \theta_2 = p_{21}m_1 \end{matrix} \quad (2)$$

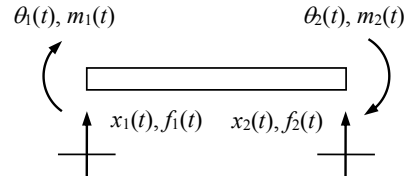


Fig. 1. Free-free beam coordinates.

Equations 1 and 2 can be written in matrix form and compactly represented using the notation shown in Eq. 3.

$$\begin{matrix} \begin{Bmatrix} x_1 \\ \theta_1 \end{Bmatrix} = \begin{bmatrix} h_{11} & l_{11} \\ n_{11} & p_{11} \end{bmatrix} \begin{Bmatrix} f_1 \\ m_1 \end{Bmatrix} \text{ or } \{u_1\} = [R_{11}]\{q_1\} \\ \begin{Bmatrix} x_2 \\ \theta_2 \end{Bmatrix} = \begin{bmatrix} h_{22} & l_{22} \\ n_{22} & p_{22} \end{bmatrix} \begin{Bmatrix} f_2 \\ m_2 \end{Bmatrix} \text{ or } \{u_2\} = [R_{22}]\{q_2\} \end{matrix} \quad (3)$$

In Eq. 3, R_{ij} is the generalized receptance matrix that describes both translational and rotational component behavior. The individual entries in these matrices include contributions from both the rigid body and flexural modes. In this study, the frequency dependent entries were calculated using the Timoshenko beam model, which includes the effects of rotary inertia and shear [85]. It was implemented using finite elements [13], where each four degree-of-freedom (rotation and displacement at each end) free-free beam section was modeled using appropriate mass and stiffness matrices [86].

These receptances can be used to couple components at their end points in order to predict assembly dynamics. For example, a free-free beam with diameter d_1 can be coupled to a second free-free beam with larger diameter d_2 to synthesize the receptances for a stepped shaft (see Fig 2). The assembly flexural receptances, shown in Eq. 4 (the upper case variables denote assembly coordinates, forces, moments, and receptances), are determined by first writing the component displacements/rotations; see Eq. 5.

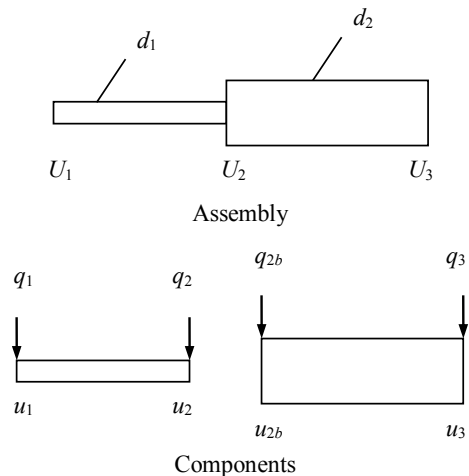


Fig. 2. Stepped shaft assembly (top) and components (bottom). Diameters d_1 and d_2 are identified in the assembly schematic.

$$\begin{Bmatrix} U_1 \\ U_2 \\ U_3 \end{Bmatrix} = \begin{bmatrix} G_{11} & G_{12} & G_{13} \\ G_{21} & G_{22} & G_{23} \\ G_{31} & G_{32} & G_{33} \end{bmatrix} \begin{Bmatrix} Q_1 \\ Q_2 \\ Q_3 \end{Bmatrix} \text{ where } U_i = \begin{Bmatrix} X_i \\ \theta_i \end{Bmatrix},$$

$$G_{ij} = \begin{bmatrix} H_{ij} & L_{ij} \\ N_{ij} & P_{ij} \end{bmatrix}, \text{ and } Q_i = \begin{Bmatrix} F_i \\ M_i \end{Bmatrix} \quad (4)$$

$$\begin{aligned} u_1 &= R_{11}q_1 + R_{12}q_2 & u_2 &= R_{21}q_1 + R_{22}q_2 \\ u_{2b} &= R_{2b2b}q_{2b} + R_{2b3}q_3 & u_3 &= R_{32b}q_{2b} + R_{33}q_3 \end{aligned} \quad (5)$$

For this stepped shaft example, a rigid connection is applied at the interface. The corresponding compatibility conditions are:

$$u_2 - u_{2b} = 0 \text{ and } u_i = U_i, \quad (6)$$

where $i = 1$ to 3 and the latter expression specifies that the component and assembly coordinates are defined at the same spatial positions. The equilibrium conditions vary with the external force/moment location. To determine the first column of the assembly receptance matrix in Eq. 4, Q_1 is applied to coordinate U_1 . In this case, the equilibrium conditions are:

$$q_2 + q_{2b} = 0, q_1 = Q_1, \text{ and } q_3 = 0. \quad (7)$$

Substitution of the component displacements/rotations and equilibrium conditions into the compatibility conditions yields q_2 ; see Eq. 8. The expression for G_{11} is then given by Eq. 9. The other two first column receptances are determined in a similar manner. To find the receptances in the second and third columns, Q_2 must be applied to U_2 and Q_3 to U_3 , respectively.

$$q_2 = -(R_{22} + R_{2b2b})^{-1}R_{21}Q_1 \quad (8)$$

$$G_{11} = \frac{U_1}{Q_1} = \frac{u_1}{Q_1} = \frac{R_{11}q_1 + R_{12}q_2}{Q_1}$$

$$G_{11} = R_{11} - R_{12}(R_{22} + R_{2b2b})^{-1}R_{21} = \begin{bmatrix} H_{11} & L_{11} \\ N_{11} & P_{11} \end{bmatrix} \quad (9)$$

In the case of finite stiffness and non-zero damping at the contact interface between components, the compatibility conditions can be modified to reflect the new coordinate displacement/rotation relationships. The Eq. 6 compatibility condition for the flexible-damped connection is now rewritten as:

$$K(u_2 - u_{2b}) = -q_{2b} \quad (10)$$

where the complex stiffness matrix is defined in Eq. 11 for a viscous damping model. In this matrix, the stiffness (k) and damping terms (c) are defined by their subscripts. The k_{xf} term, for example, describes the stiffness that relates force to displacement, while the stiffness $k_{\theta m}$ relates rotation to moment.

$$K = \begin{bmatrix} k_{xf} + i\omega c_{xf} & k_{\theta f} + i\omega c_{\theta f} \\ k_{xm} + i\omega c_{xm} & k_{\theta m} + i\omega c_{\theta m} \end{bmatrix} \quad (11)$$

Using the Eq. 10 compatibility condition, the assembly receptance from Eq. 9 is modified to be:

$$G_{11} = R_{11} - R_{12}(R_{22} + R_{2b2b} + K^{-1})^{-1}R_{21}. \quad (12)$$

For tool point receptance predictions, coordinates 1 and 2 in Eq. 12 are defined by the two ends of the holder-tool model, while coordinate 2b is associated with the machine-spindle. To experimentally identify the R_{2b2b} receptances, a standard artifact with the appropriate spindle-holder connection (e.g., CAT-40 or HSK-63A) is inserted in the spindle under test. The four direct receptances at the free end of the artifact are determined from a single displacement-to-force measurement as described in [22]. The machine-spindle receptances are then determined from the machine-spindle-artifact receptances using the inverse RCSA approach detailed in [13]. In this method, the assembly receptances are measured and then the free-free portion of the artifact beyond the holder flange is extracted to isolate the machine-spindle receptances; see Fig. 3.

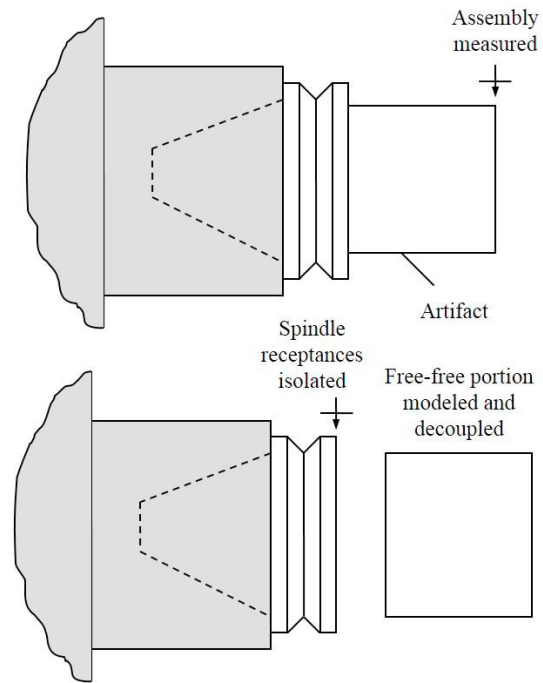


Fig. 3. Machine-spindle receptances are determined using inverse RCSA.

3. Tool point receptance results

The RCSA approach was used to predict the tool point receptances for various tool extension lengths. The first step was to determine the machine-spindle receptances using inverse RCSA as described in Section 2. The artifact measurement for a selected CNC milling machine spindle (CAT-40 spindle-holder connection) is displayed in Fig. 4. Multiple vibration modes appear in the 5000 Hz measurement bandwidth. The measurement was completed using a PCB 086C03 modal hammer, PCB 352C23 low-mass accelerometer, and MLI's MetalMax TXF software.

The portion of the cylindrical steel artifact (200 GPa modulus, 7800 kg/m³ density, 0.29 Poisson's ratio) beyond the flange was then extracted to isolate the machine-spindle receptances. The 52.5 mm outer diameter cylinder had a length of 59.9 mm with an internal diameter of 29.9 mm to a depth of

40 mm. The displacement-to-force result is shown in Fig. 5 (dotted line). The original artifact receptance is also included (solid line) to demonstrate that removal of the mass beyond the flange serves to increase the natural frequencies and reduce the magnitudes of individual modes. It is important to note that this response serves as the “boundary condition” for the free-free holder-tool receptances which are coupled to the machine-spindle to predict the assembly dynamics. These dynamics are then available to predict the milling performance and selection optimized parameters for maximum material removal rate (*MRR*).

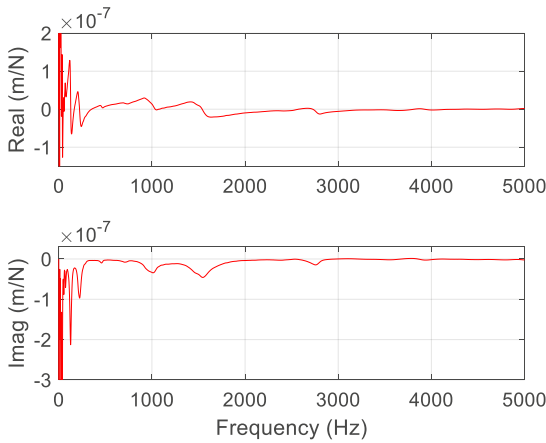


Fig. 4. Measured machine-spindle-artifact displacement-to-force receptance.

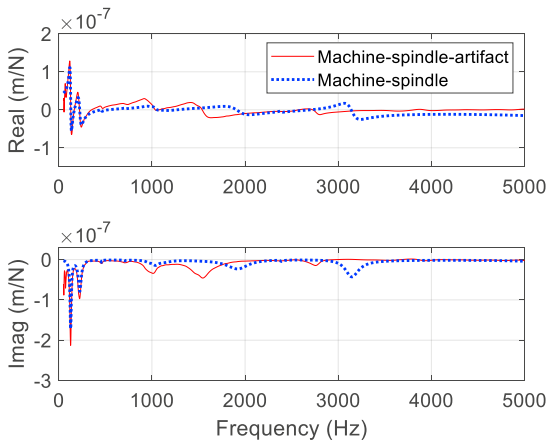


Fig. 5. Machine-spindle displacement-to-force receptance (dotted line) compared to machine-spindle-artifact receptance (solid line).

Once the machine-spindle receptances were archived, the holder and tool receptances were next computed using the Timoshenko beam model. A 50 mm outer diameter, steel stub length thermal shrink fit holder (CAT-40 spindle interface, 40 mm length with 12 mm internal diameter) was selected to clamp 12 mm diameter carbide rods (550 GPa modulus, 15000 kg/m³ density, 0.22 Poisson’s ratio). In each case, the insertion length was 20 mm. An example tool point FRF measurement and RCSA prediction is displayed in Fig. 6, where the tool

extension length was 40 mm. The connection matrix between the tool and holder, which represents the non-rigid shrink fit holder-tool connection, is provided in Eq. 13. Figure 6 shows a single, dominant holder-tool bending mode at 3809 Hz.

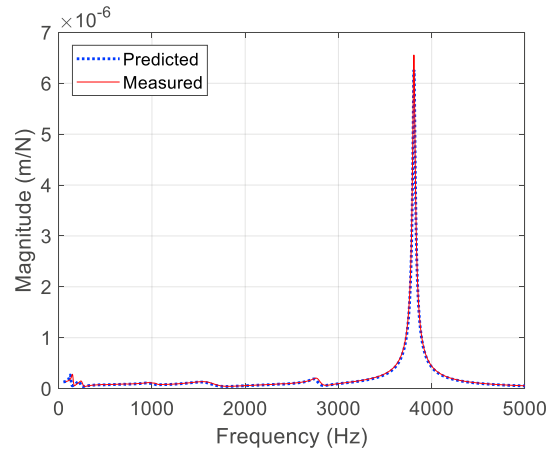


Fig. 6. Predicted (dotted line) and measured (solid line) tool point FRFs for 40 mm extension length.

$$K = \begin{bmatrix} 5 \times 10^7 \frac{N}{m} & 0 \\ 0 & 5 \times 10^5 \frac{rad}{N-m} \end{bmatrix} \quad (13)$$

Figure 7 displays the tool point FRF for a 50 mm extension. The anticipated response is single mode with a larger magnitude and lower frequency than Fig. 6. However, the Fig. 7 result demonstrates an interaction between the holder-tool bending mode and a machine-spindle mode. This produces a response dominated by two modes, rather than one. The machine-spindle effectively acts as a dynamic absorber for the holder-tool. Some of the energy that would typically go toward producing the tool point response now escapes through the spindle and into the machine. The dynamic stiffness is therefore higher for the new two-mode FRF.

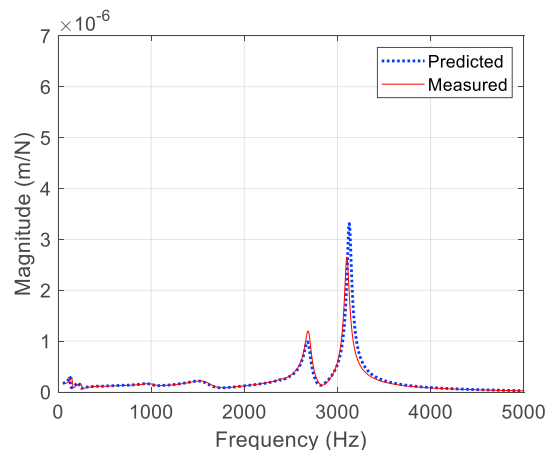


Fig. 7. Predicted (dotted line) and measured (solid line) tool point FRFs for 50 mm extension length (same scale as Fig. 6).

To emphasize the holder-tool bending mode interaction with the machine-spindle mode, Fig. 8 is provided. A semi-log scale was selected to enable the machine-spindle, 40 mm extension, and 50 mm extension FRFs to be viewed simultaneously. It is observed that the 50 mm extension causes the holder-tool mode to interact with the machine-spindle mode at 3155 Hz. In the same way as a dynamic absorber, matching the natural frequencies of the two systems produces a new two-mode combined system with increased dynamic stiffness (reduced magnitude).

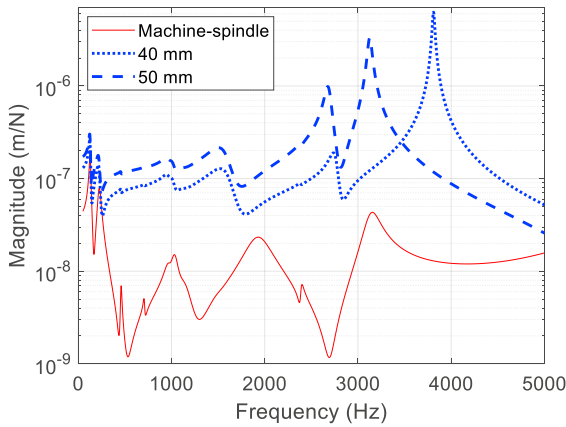


Fig. 8. Comparison of machine-spindle (solid line), 40 mm tool extension (dotted line), and 50 mm tool extension (dashed line) FRFs.

4. Stability implications

A comparison of tool point predictions is provided in Fig. 9. Four extension lengths were selected: {40, 50, 60, and 70} mm. The results are counter-intuitive. The shortest extension length gives the largest magnitude. This is because there are no spindle modes near the holder-tool bending frequency. The interaction with the 3155 Hz machine-spindle mode increases the dynamic stiffness for the 50 mm extension. A reduced interaction for the 60 mm extension causes the magnitude to increase relative to the 50 mm extension, as expected. However, the 70 mm extension offers the highest dynamic stiffness due to a strong interaction with the highly damped 1930 Hz machine-spindle mode (see Fig. 8).

Using the predictive RCSA capability, a plot of the peak magnitude value for each tool point FRF over a range of extension lengths can be produced. Figure 10 displays the peak tool point magnitudes for lengths from 30 mm to 90 mm for two cases: 1) the measured machine-spindle receptances serve as the base for the holder model (rigid connection), which is then coupled to the tool model (flexible connection); and 2) a rigid base is coupled to the tool holder (rigid connection), which is then coupled to the tool model (flexible connection). It is seen that the magnitudes differ substantially. The rigid base results are, surprisingly, much more flexible. This is because the shrink fit holder and carbide rods offer little damping. The majority of the assembly damping comes from the machine-spindle dynamics. For this reason, the machine-spindle-holder-tool coupling results offer much higher dynamic stiffness.

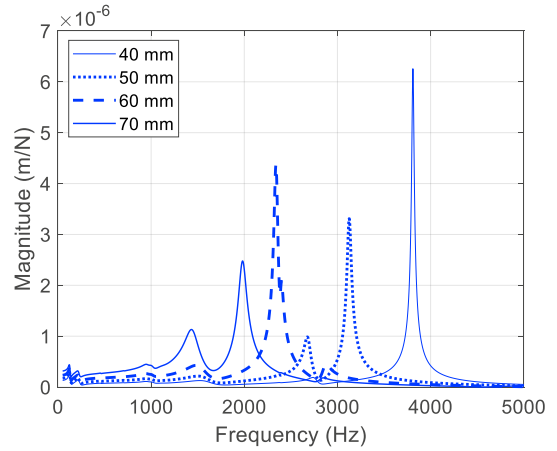


Fig. 9. Comparison of tool point FRFs for four tool extension lengths.

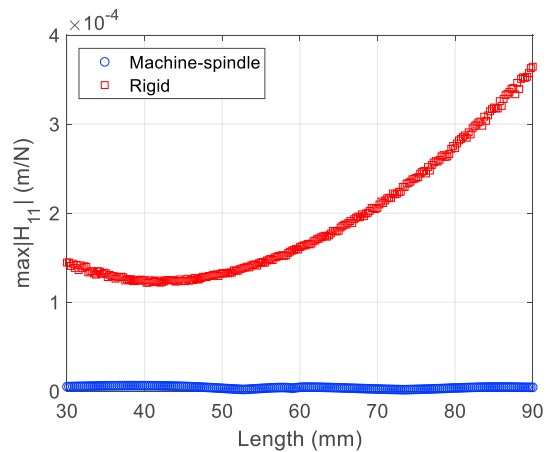


Fig. 10. Comparison of maximum tool point FRF magnitudes for two cases: holder and tool coupled to machine-spindle (blue circles); and holder and tool coupled to rigid base (red squares).

The interested reader might also notice that there is apparent “noise” superimposed on the rigid based coupling results in Fig. 10. This is due to the very light damping for these receptances. When combined with the discrete sampling frequency, the narrow peak is not always exactly captured by the predicted FRF. Also, the maximum magnitude does not monotonically increase because the tool is flexibly coupled to the non-rigid holder. When the tool length is small, its stiffness is similar to the holder stiffness and the local decrease, followed by the monotonic increase is obtained.

The rigid result from Fig. 10 is removed in Fig. 11 to emphasize the machine-spindle and holder-tool interactions. These results mimic Fig. 9. Increased dynamic stiffness is observed at locations where the holder-tool bending natural frequency is near a spindle natural frequency. As seen in Fig. 9, a large maximum magnitude occurs for a 40 mm extension, a much smaller result is obtained for 50 mm, the magnitude increases from 50 mm to 60 mm, and then the smallest magnitude for these four extension lengths is observed at 70 mm.

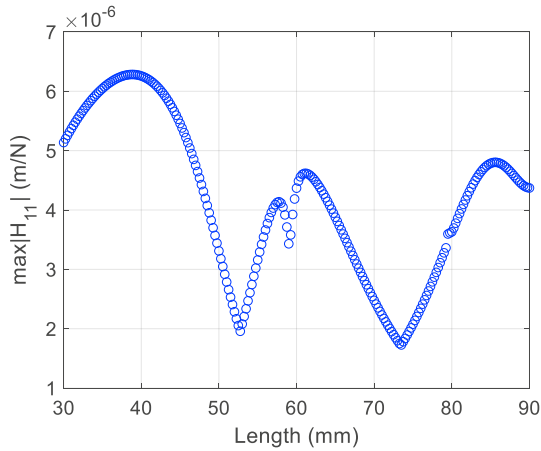


Fig. 11. Comparison of maximum tool point FRF magnitudes for holder and tool coupled to machine-spindle.

While the variation in tool point FRF with extension length and machine-spindle interactions is interesting, the more important implication is the influence on milling stability. To explore this sensitivity, stability maps were computed for each extension length. The analytical solution presented by Altintas and Budak [87] was applied with a 6061-T6 aluminum work material (750 N/mm² specific cutting force and 68 deg force angle), a 12 mm diameter endmill with four teeth, and 25% radial immersion down milling. Example results are displayed in Fig. 12 for extension lengths of 40 mm and 70 mm (similar to Fig. 9). It is seen that the lightly damped, larger magnitude 40 mm extension response gives narrow stability zones with a critical stability limit (i.e., axial depth that is stable for all spindle speeds) of 0.65 mm. The smaller magnitude response with increased damping for the 70 mm extension gives wider stability zones and a critical stability limit of 1.54 mm. The increased damping also changes the slope of the stability boundary, so that the wider zones do not extend as far vertically as the more lightly damped zones for the 40 mm extension.

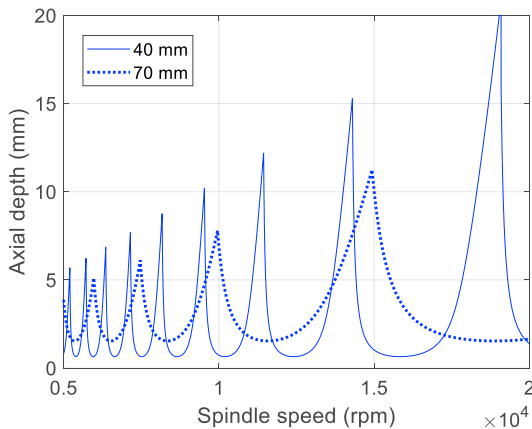


Fig. 12. Stability maps for 40 mm extension (solid line) and 70 mm extension (dotted line).

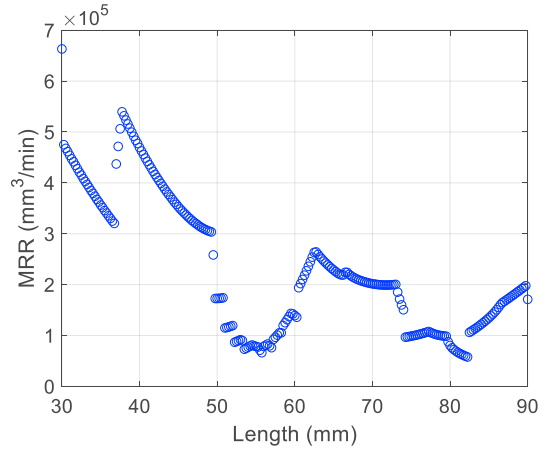


Fig. 13. Mean MRR as a function of extension length.

To compare the stability behavior over the full range of extension lengths in Fig. 11 (30 mm to 90 mm), the following procedure was applied.

1. An extension length was selected and the tool point FRF was calculated.
2. This FRF was used to compute the stability map (25% radial immersion down milling, four teeth, 6061-T6 aluminum workpiece).
3. The maximum stable axial depth of cut was identified from the stability boundary and the corresponding spindle speed was recorded.
4. The mean material removal rate for this spindle speed-axial depth pair was calculated using Eq. 16, where $\max b_{lim}$ (mm) is the maximum value from the stability boundary, $\Omega_{b=\max b_{lim}}$ (rpm) is the corresponding spindle speed, the feed per tooth was 0.1 mm, the radial depth was 3 mm, and there were four teeth on the endmill.

$$MRR = \max b_{lim} (3)(0.1)(4)\Omega_{b=\max b_{lim}} \quad (14)$$

The results are presented in Fig. 13. It is seen that there is a local decrease in MRR at the same locations where the interactions between machine-spindle and holder-tool modes occur (see the local minima in Fig. 11). As discussed in Fig. 12, this is because the increased damping in the two mode “interaction responses” causes the peak heights of the stable zones to be truncated, even though the critical stability limit is increased. However, the maximum stable axial depths obtained from Fig. 13 for use in Eq. 14 were selected without regard to the sensitivity of the peak points. For example, for the rightmost stable zone in Fig. 12 corresponding to the 40 mm extension (solid line), it is most likely not feasible to choose an axial depth of 20 mm due to modeling uncertainties and inherent process variations. Within that stable zone, a maximum depth of 10 mm (or less) might be selected by a risk adverse process planner. It is therefore a user-dependent evaluation as to whether the increased dynamic stiffness offered by the interactions between the machine-spindle and holder-tool modes is desirable or not.

5. Summary

This paper implemented receptance coupling substructure analysis (RCSA) to predict tool point receptances for a range of extension lengths with holder-tool bending modes that spanned multiple machine-spindle bending modes for a selected CNC milling machine. It was shown that the holder-tool modes interacted with the machine-spindle modes to yield increased dynamic stiffness for selected extension lengths. The implications of these variations in dynamic stiffness on milling stability were then discussed.

To explore the effect on milling performance, stability maps were computed for a range of tool extension lengths. It was seen that the lightly damped, larger magnitude responses where no interaction occurred provided more narrow stability zones and lower critical stability limits. The smaller magnitude responses with increased damping obtained for tool extensions that resulted in interaction with the machine-spindle modes gave wider stability zones and larger critical stability limits. The increased damping also changed the slope of the stability boundary, so that the wider zones did not extend as far vertically as the more lightly damped zones. This provides a tradeoff between modeling and process uncertainty and potentially higher material removal rates. Ultimately, the research shows that it is important to consider the entire machine-spindle-holder-tool assembly when selecting machining parameters and assessing the material removal performance.

Acknowledgements

The author gratefully acknowledges financial support from the National Science Foundation (CMMI-1561221) and Oak Ridge National Laboratory.

References

- [1] Ewins, D.J., 1984. Modal testing: Theory and practice (Vol. 15). Letchworth: Research Studies Press.
- [2] Schmitz, T.L. and Smith, K.S., 2019. Machining dynamics: Frequency response to improved productivity, 2nd Ed. Springer, New York.
- [3] Honeycutt, A. and Schmitz, T., 2018. Milling bifurcations: A review of literature and experiment. *Journal of Manufacturing Science and Engineering*, 140(12), 120801.
- [4] Altıntaş, Y., 2000. Manufacturing automation. Cambridge University Press, New York.
- [5] Schmitz, T.L. and Donaldson, R.R., 2000. Predicting high-speed machining dynamics by substructure analysis. *CIRP Annals-Manufacturing Technology*, 49(1), pp. 303-308.
- [6] Schmitz, T., Davies, M. and Kennedy, M., 2000, July. High-speed machining frequency response prediction for process optimization. In *Proceedings of the 2nd International Seminar on Improving Machine Tool Performance*, La Baule, France (pp. 3-5).
- [7] Schmitz, T.L., Davies, M.A. and Kennedy, M.D., 2001. Tool point frequency response prediction for high-speed machining by RCSA. *Journal of Manufacturing Science and Engineering*, 123(4), pp. 700-707.
- [8] Schmitz, T.L., Davies, M.A., Medicus, K. and Snyder, J., 2001. Improving high-speed machining material removal rates by rapid dynamic analysis. *CIRP Annals-Manufacturing Technology*, 50(1), pp. 263-268.
- [9] Schmitz, T. and Burns, T., 2003, February. Receptance coupling for high-speed machining dynamics prediction. In *Proceedings of the 21st International Modal Analysis Conference (Vol. 36)*.
- [10] Schmitz, T.L., Burns, T.J., Ziegert, J.C., Dutterer, B. and Winfough, W.R., 2004. Tool length-dependent stability surfaces. *Machining Science and Technology*, 8(3), pp. 377-397.
- [11] Burns, T.J. and Schmitz, T.L., 2004, January. Receptance coupling study of tool-length dependent dynamic absorber effect. In *ASME 2004 International Mechanical Engineering Congress and Exposition (pp. 993-1000)*. American Society of Mechanical Engineers.
- [12] Schmitz, T.L., 2004, January. Improved sensor data utility through receptance coupling modeling. In *ASME 2004 International Mechanical Engineering Congress and Exposition (pp. 411-417)*. American Society of Mechanical Engineers.
- [13] Schmitz, T.L. and Duncan, G.S., 2005. Three-component receptance coupling substructure analysis for tool point dynamics prediction. *Journal of Manufacturing Science and Engineering*, 127(4), pp. 781-790.
- [14] Burns, T.J. and Schmitz, T.L., 2005, January. A study of linear joint and tool models in spindle-holder-tool receptance coupling. In *ASME 2005 International Design Engineering Technical Conferences and Computers and Information in Engineering Conference (pp. 947-954)*. American Society of Mechanical Engineers.
- [15] Duncan, G.S., Tummond, M.F. and Schmitz, T.L., 2005. An investigation of the dynamic absorber effect in high-speed machining. *International Journal of Machine Tools and Manufacture*, 45(4-5), pp. 497-507.
- [16] Duncan, G.S. and Schmitz, T., 2005, January. An improved RCSA model for tool point frequency response prediction. In *Proceedings of the 23rd International Modal Analysis Conference (Vol. 30)*.
- [17] Cheng, C.H., Schmitz, T.L., Arakere, N. and Duncan, G.S., 2005, January. An approach for micro end mill frequency response predictions. In *ASME 2005 International Mechanical Engineering Congress and Exposition (pp. 1139-1145)*. American Society of Mechanical Engineers.
- [18] Schmitz, T.L. and Duncan, G.S., 2006. Receptance coupling for dynamics prediction of assemblies with coincident neutral axes. *Journal of Sound and Vibration*, 289(4-5), pp. 1045-1065.
- [19] Schmitz, T.L., Powell, K., Won, D., Duncan, G.S., Sawyer, W.G. and Ziegert, J.C., 2007. Shrink fit tool holder connection stiffness/damping modeling for frequency response prediction in milling. *International Journal of Machine Tools and Manufacture*, 47(9), pp. 1368-1380.
- [20] Cheng, C.H., Schmitz, T.L. and Scott Duncan, G., 2007. Rotating tool point frequency response prediction using RCSA. *Machining Science and Technology*, 11(3), pp. 433-446.
- [21] Schmitz, T.L., 2010. Torsional and axial frequency response prediction by RCSA. *Precision Engineering*, 34(2), pp. 345-356.
- [22] Kumar, U.V. and Schmitz, T.L., 2012. Spindle dynamics identification for receptance coupling substructure analysis. *Precision Engineering*, 36(3), pp. 435-443.
- [23] Honeycutt, A. and Schmitz, T., 2018. Receptance coupling model for variable dynamics in fixed-free thin rib machining. *Procedia Manufacturing*, 26, pp. 173-180.
- [24] Schmitz, T., Honeycutt, A., Gomez, M., Stokes, T.M., and Betters, E., 2019. Multi-point coupling for tool point receptance prediction. *Journal of Manufacturing Processes*, 43, pp. 2-11.
- [25] Park, S.S., Altıntaş, Y. and Movahhedy, M., 2003. Receptance coupling for end mills. *International Journal of Machine Tools and Manufacture*, 43(9), pp. 889-896.
- [26] Kivanc, E.B. and Budak, E., 2004. Structural modeling of end mills for form error and stability analysis. *International Journal of Machine Tools and Manufacture*, 44(11), pp. 1151-1161.
- [27] Ertürk, A., Özgüven, H.N. and Budak, E., 2006. Analytical modeling of spindle-tool dynamics on machine tools using Timoshenko beam model and receptance coupling for the prediction of tool point FRF. *International Journal of Machine Tools and Manufacture*, 46(15), pp. 1901-1912.
- [28] Ertürk, A., Özgüven, H. and Budak, E., 2006. Analytical modeling of spindle-tool dynamics on machine tools using Timoshenko beam model and receptance coupling for the prediction of tool point FRF. *International Journal of Machine Tools and Manufacture*, 46(15).
- [29] Budak, E., Ertürk, A. and Özgüven, H.N., 2006. A modeling approach for analysis and improvement of spindle-holder-tool assembly dynamics. *CIRP Annals-Manufacturing Technology*, 55(1), pp. 369-372.

- [30] Park, S.S., 2006. Identification of spindle integrated force sensor's transfer function for modular end mills. *Journal of Manufacturing Science and Engineering*, 128(1), pp. 146-153.
- [31] Movahhedy, M.R. and Gerami, J.M., 2006. Prediction of spindle dynamics in milling by sub-structure coupling. *International Journal of Machine Tools and Manufacture*, 46(3-4), pp. 243-251.
- [32] Ertürk, A., Budak, E. and Özgüven, H.N., 2007. Selection of design and operational parameters in spindle-holder-tool assemblies for maximum chatter stability by using a new analytical model. *International Journal of Machine Tools and Manufacture*, 47(9), pp. 1401-1409.
- [33] Namazi, M., Altintas, Y., Abe, T. and Rajapakse, N., 2007. Modeling and identification of tool holder-spindle interface dynamics. *International Journal of Machine Tools and Manufacture*, 47(9), pp. 1333-1341.
- [34] Ahmadi, K. and Ahmadian, H., 2007. Modelling machine tool dynamics using a distributed parameter tool-holder joint interface. *International Journal of Machine Tools and Manufacture*, 47(12-13), pp. 1916-1928.
- [35] Ertürk, A., Özgüven, H.N. and Budak, E., 2007. Effect analysis of bearing and interface dynamics on tool point FRF for chatter stability in machine tools by using a new analytical model for spindle-tool assemblies. *International Journal of Machine Tools and Manufacture*, 47(1), pp. 23-32.
- [36] Houming, Z., Chengyong, W. and Zhenyu, Z., 2008. Dynamic characteristics of conjunction of lengthened shrink-fit holder and cutting tool in high-speed milling. *Journal of Materials Processing Technology*, 207(1-3), pp. 154-162.
- [37] Park, S.S. and Chae, J., 2008. Joint identification of modular tools using a novel receptance coupling method. *The International Journal of Advanced Manufacturing Technology*, 35(11-12), pp. 1251-1262.
- [38] Mascardelli, B.A., Park, S.S. and Freiheit, T., 2008. Substructure coupling of microend mills to aid in the suppression of chatter. *Journal of Manufacturing Science and Engineering*, 130(1), p. 011010.
- [39] Özşahin, O., Ertürk, A., Özgüven, H.N. and Budak, E., 2009. A closed-form approach for identification of dynamical contact parameters in spindle-holder-tool assemblies. *International Journal of Machine Tools and Manufacture*, 49(1), pp. 25-35.
- [40] Banerjee, A., Bordatchev, E.V. and Feng, H.Y., 2009. Determination of minimum limiting axial depth of cut for 2½D pocket machining based on receptance coupling. *Machining Science and Technology*, 13(2), pp. 177-195.
- [41] Mancisidor, I., Zatarain, M., Munoa, J. and Dombovari, Z., 2011. Fixed boundaries receptance coupling substructure analysis for tool point dynamics prediction. In *Advanced Materials Research* (Vol. 223, pp. 622-631). Trans Tech Publications.
- [42] Mancisidor, I., Zatarain, M., Munoa, J. and Dombovari, Z., 2011, May. Receptance coupling for tool point dynamics prediction. In *17th CIRP International Conference on Modelling of Machining Operations*.
- [43] Kolar, P., Sulitka, M. and Janota, M., 2011. Simulation of dynamic properties of a spindle and tool system coupled with a machine tool frame. *The International Journal of Advanced Manufacturing Technology*, 54(1-4), pp. 11-20.
- [44] Forestier, F., Gagnol, V., Ray, P. and Paris, H., 2011. Model-based operating recommendations for high-speed spindles equipped with a self-vibratory drilling head. *Mechanism and Machine Theory*, 46(11), pp. 1610-1622.
- [45] Mehrpouya, M. and Park, S.S., 2011. Prediction of atomic force microscope probe dynamics through the receptance coupling method. *Review of Scientific Instruments*, 82(12), p. 125001.
- [46] Rezaei, M.M., Movahhedy, M.R., Moradi, H. and Ahmadian, M.T., 2012. Extending the inverse receptance coupling method for prediction of tool-holder joint dynamics in milling. *Journal of Manufacturing Processes*, 14(3), pp. 199-207.
- [47] Albertelli, P., Cau, N., Bianchi, G. and Monno, M., 2012. The effects of dynamic interaction between machine tool subsystems on cutting process stability. *The International Journal of Advanced Manufacturing Technology*, 58(9-12), pp. 923-932.
- [48] Cao, H., Li, B. and He, Z., 2013. Finite element model updating of machine-tool spindle systems. *Journal of Vibration and Acoustics*, 135(2), p. 024503.
- [49] Albertelli, P., Goletti, M. and Monno, M., 2013. A new receptance coupling substructure analysis methodology to improve chatter free cutting conditions prediction. *International Journal of Machine Tools and Manufacture*, 72, pp. 16-24.
- [50] Wang, E., Wu, B., Hu, Y., Yang, S. and Cheng, Y., 2013. Dynamic parameter identification of tool-spindle interface based on RCSA and particle swarm optimization. *Shock and Vibration*, 20(1), pp. 69-78.
- [51] Mehrpouya, M., Graham, E. and Park, S.S., 2013. FRF based joint dynamics modeling and identification. *Mechanical Systems and Signal Processing*, 39(1-2), pp. 265-279.
- [52] Xu, C., Zhang, J., Wu, Z., Yu, D. and Feng, P., 2013. Dynamic modeling and parameters identification of a spindle-holder taper joint. *The International Journal of Advanced Manufacturing Technology*, 67(5-8), pp. 1517-1525.
- [53] Albertelli, P., Goletti, M. and Monno, M., 2013. An improved receptance coupling substructure analysis to predict chatter free high speed cutting conditions. *Procedia CIRP*, 12, pp. 19-24.
- [54] Brecher, C., Bäuml, S. and Daniels, M., 2014. Prediction of dynamics of modified machine tool by experimental substructuring. In *Dynamics of Coupled Structures*, Volume 1 (pp. 297-305). Springer, Cham.
- [55] Mancisidor, I., Urkiola, A., Barcena, R., Munoa, J., Dombovari, Z. and Zatarain, M., 2014. Receptance coupling for tool point dynamic prediction by fixed boundaries approach. *International Journal of Machine Tools and Manufacture*, 78, pp. 18-29.
- [56] Mehrpouya, M., Graham, E. and Park, S.S., 2015. Identification of multiple joint dynamics using the inverse receptance coupling method. *Journal of vibration and control*, 21(16), pp. 3431-3449.
- [57] Grossi, N., Montevecchi, F., Scippa, A. and Campatelli, G., 2015. 3D finite element modeling of holder-tool assembly for stability prediction in milling. *Procedia CIRP*, 31, pp. 527-532.
- [58] Xu, C., Zhang, J., Yu, D., Wu, Z. and Feng, P., 2015. Dynamics prediction of spindle system using joint models of spindle tool holder and bearings. *Proceedings of the Institution of Mechanical Engineers, Part C: Journal of Mechanical Engineering Science*, 229(17), pp. 3084-3095.
- [59] Özşahin, O., Budak, E. and Özgüven, H.N., 2015. Identification of bearing dynamics under operational conditions for chatter stability prediction in high speed machining operations. *Precision Engineering*, 42, pp. 53-65.
- [60] Cao, H., Xi, S. and Cheng, W., 2015. Model updating of spindle systems based on the identification of joint dynamics. *Shock and Vibration*, 2015.
- [61] Yang, Y., Wan, M., Ma, Y.C. and Zhang, W.H., 2016. An improved method for tool point dynamics analysis using a bi-distributed joint interface model. *International Journal of Mechanical Sciences*, 105, pp. 239-252.
- [62] Mehrpouya, M., Sanati, M. and Park, S.S., 2016. Identification of joint dynamics in 3D structures through the inverse receptance coupling method. *International Journal of Mechanical Sciences*, 105, pp. 135-145.
- [63] Liu, H., Lu, D., Zhang, J. and Zhao, W., 2016. Receptance coupling of multi-subsystem connected via a wedge mechanism with application in the position-dependent dynamics of ballscrew drives. *Journal of Sound and Vibration*, 376, pp. 166-181.
- [64] Grossi, N., Sallè, L., Montevecchi, F., Scippa, A. and Campatelli, G., 2016. Speed-varying machine tool dynamics identification through chatter detection and receptance coupling. *Procedia CIRP*, 55, pp. 77-82.
- [65] Grossi, N., Scippa, A., Montevecchi, F. and Campatelli, G., 2016. A novel experimental-numerical approach to modeling machine tool dynamics for chatter stability prediction. *Journal of Advanced Mechanical Design, Systems, and Manufacturing*, 10(2), pp. JAMDSM0019-JAMDSM0019.
- [66] Brecher, C., Chavan, P., Fey, M. and Daniels, M., 2016. A modal parameter approach for receptance coupling of tools. *MM Science Journal*, pp. 1032-1034.
- [67] Montevecchi, F., Grossi, N., Scippa, A. and Campatelli, G., 2016. Improved RCSA technique for efficient tool-tip dynamics prediction. *Precision Engineering*, 44, pp. 152-162.
- [68] Matthias, W., Özşahin, O., Altintas, Y. and Denkena, B., 2016. Receptance coupling based algorithm for the identification of contact parameters at holder-tool interface. *CIRP Journal of Manufacturing Science and Technology*, 13, pp. 37-45.
- [69] Zhao, Y., Song, X., Cai, L., Liu, Z. and Cheng, Q., 2016. Surface fractal topography-based contact stiffness determination of spindle-toolholder joint. *Proceedings of the Institution of Mechanical Engineers, Part C: Journal of Mechanical Engineering Science*, 230(4), pp. 602-610.

- [70] Xu, C., Feng, P., Zhang, J., Yu, D. and Wu, Z., 2017. Milling stability prediction for flexible workpiece using dynamics of coupled machining system. *The International Journal of Advanced Manufacturing Technology*, 90(9-12), pp. 3217-3227.
- [71] Montevocchi, F., Grossi, N., Scippa, A. and Campatelli, G., 2017. Two-points-based receptance coupling method for tool-tip dynamics prediction. *Machining Science and Technology*, 21(1), pp. 136-156.
- [72] Xiaohong, L., Zhenyuan, J., Haixing, Z., Shengqian, L., Yixuan, F. and Liang, S.Y., 2017. Tool Point Frequency Response Prediction for Micromilling by Receptance Coupling Substructure Analysis. *Journal of Manufacturing Science and Engineering*, 139(7), p. 071004.
- [73] Qi, B., Sun, Y. and Li, Z., 2017. Tool point frequency response function prediction using RCSA based on Timoshenko beam model. *The International Journal of Advanced Manufacturing Technology*, 92(5-8), pp. 2787-2799.
- [74] Jasiewicz, M. and Powalka, B., 2018. Identification of a Lathe Spindle Dynamics Using Extended Inverse Receptance Coupling. *Journal of Dynamic Systems, Measurement, and Control*, 140(12), p. 121015.
- [75] Özşahin, O., 2018. Determination of tool point FRF of micro tools under operational conditions using analytical methods. *Journal of the Faculty of Engineering and Architecture of Gazi University*, 33(2), pp. 529-539.
- [76] Singh, K.K., Kulkarni, S.S., Kartik, V. and Singh, R., 2018. A Free Interface Component Mode Synthesis Approach for Determining the Micro-end Mill Dynamics. *Journal of Micro and Nano-Manufacturing*, 6(3), p. 031005.
- [77] Postel, M., Özşahin, O. and Altintas, Y., 2018. High speed tooltip FRF predictions of arbitrary tool-holder combinations based on operational spindle identification. *International Journal of Machine Tools and Manufacture*, 129, pp. 48-60.
- [78] Ealo, J.A., Garitaonandia, I., Fernandes, M.H., Hernandez-Vazquez, J.M. and Muñoa, J., 2018. A practical study of joints in three-dimensional Inverse Receptance Coupling Substructure Analysis method in a horizontal milling machine. *International Journal of Machine Tools and Manufacture*, 128, pp. 41-51.
- [79] Li, Z., Wang, Z., Shi, X. and Li, W., 2018. RCSA-based prediction of chatter stability for milling process with large axial depth of cut. *The International Journal of Advanced Manufacturing Technology*, 96(1-4), pp. 833-843.
- [80] Shaik, J.H., Ramakotaiyah, K. and Srinivas, J., 2018. Frequency Response Studies using Receptance Coupling Approach in High Speed Spindles. *Journal of The Institution of Engineers (India): Series C*, pp. 1-12.
- [81] Jasiewicz, M. and Powalka, B., 2018, January. Prediction of turning stability using receptance coupling. In *AIP Conference Proceedings* (Vol. 1922, No. 1, p. 100005). AIP Publishing.
- [82] Ji, Y., Bi, Q., Zhang, S. and Wang, Y., 2018. A new receptance coupling substructure analysis methodology to predict tool tip dynamics. *International Journal of Machine Tools and Manufacture*, 126, pp. 18-26.
- [83] Tunc, L.T., 2018. Prediction of tool tip dynamics for generalized milling cutters using the 3D model of the tool body. *The International Journal of Advanced Manufacturing Technology*, 95(5-8), pp. 1891-1909.
- [84] Liao, J., Yu, D., Zhang, J., Feng, P. and Wu, Z., 2018. An efficient experimental approach to identify tool point FRF by improved receptance coupling technique. *The International Journal of Advanced Manufacturing Technology*, 94(1-4), pp. 1451-1460.
- [85] Weaver, Jr., W., Timoshenko, P., and Young, D., 1990. *Vibration problems in engineering*, 5th Ed. John Wiley and Sons, New York.
- [86] Yokoyama, T., 1990. Vibrations of a hanging Timoshenko beam under gravity. *Journal of Sound and Vibration*, 141, pp. 245-258.
- [87] Altıntaş, Y. and Budak, E., 1995. Analytical prediction of stability lobes in milling. *CIRP Annals*, 44(1), pp.357-362.